

A new class of chimeras in locally coupled oscillators with small-amplitude, high-frequency asynchrony and large-amplitude, low-frequency synchrony

Tasso J. Kaper^{1, a)} and Theodore Vo^{2, b)}

¹⁾*Department of Mathematics and Statistics, Boston University, Boston, MA 02215, USA*

²⁾*School of Mathematics, Monash University, Clayton, Victoria 3800, Australia*

(Dated: 17 August 2021)

Chimeras are surprising yet important states in which domains of decoherent (asynchronous) and coherent (synchronous) oscillations co-exist. In this article, we report on the discovery of a new class of chimeras, called *mixed-amplitude chimera states*, in which the structures, amplitudes, and frequencies of the oscillations differ substantially in the decoherent and coherent regions. These mixed-amplitude chimeras exhibit domains of decoherent small-amplitude oscillations (phase waves) coexisting with domains of stable and coherent large-amplitude or mixed-mode oscillations. They are observed in a prototypical bistable partial differential equation with spatially homogeneous kinetics and purely local, isotropic diffusion. New bifurcations are identified in which the mixed-amplitude chimeras emerge from, or are annihilated in, common large-amplitude solutions. Also, key singularities, folded nodes and folded saddles, arising commonly in multi-scale, bistable systems play important roles, and these have not previously been studied in systems with chimeras. The discovery of these mixed-amplitude chimeras is an important advance for understanding some processes in neuroscience, pattern formation, and physics which involve both small-amplitude and large-amplitude oscillations. It may also be of use for understanding some aspects of EEG recordings from animals that exhibit unihemispheric slow-wave sleep.

A striking phenomenon in pattern formation occurs when groups of identical oscillators exhibit domains of decoherent oscillations coexisting with complementary domains of coherent dynamics. These states are known as chimera states, named after animals from Greek mythology, which have body parts from different known animals. However, unlike the mythological beasts, chimera states arise ubiquitously in many areas of physics, chemistry, neuroscience, and engineering. This article reports on the discovery of a completely new class of chimeras. The structures, amplitudes, and frequencies of the oscillations differ substantially in the decoherent and coherent domains. Underlying these chimeras are folded singularities, which are well-known to be generating mechanisms for complex oscillatory dynamics. The discovery of this new class of chimeras was made on a proto-typical bistable partial differential equation. These new chimeras have the potential to make useful applications, including to unihemispheric slow wave sleep, during which the sleeping cerebral hemisphere exhibits synchronous high-amplitude, low-frequency rhythms characteristic of sleep, while the other hemisphere displays the decoherent low-amplitude, high-frequency rhythms characteristic of wakefulness.

I. INTRODUCTION

Discovered in rings of identical phase oscillators^{1,2}, chimera states are fascinating patterns which exhibit coexisting domains of decoherent (asynchronous) and coherent (synchronous) oscillations. They occur broadly in models and experiments in physics, neuroscience, chemistry, and biology, including in systems of coupled oscillators, integro-differential equations, and partial differential equations^{3–29}. Coupling of the identical systems may be non-local, global, local, or via delay or noise. Reviews and classifications are given in Refs. 18, 20, and 24.

In this article, we report on a new class of chimeras – *mixed-amplitude chimeras* – which exhibit regions of decoherent small-amplitude oscillations (SAOs) and complementary regions of coherent large-amplitude relaxation oscillations (LAOs) or coherent mixed-mode oscillations (MMOs). (The latter are combinations of LAOs and SAOs^{30–34}.) The decoherent and coherent dynamics differ qualitatively and quantitatively, with amplitudes separated by at least one order of magnitude and frequencies widely separated. The SAOs are phase waves of high frequency, whereas the LAOs and MMOs jump between distinct states and are of low frequency.

The existence of mixed-amplitude chimeras is surprising, since the LAOs and MMOs are robust states in bistable systems. Also, as shown here, in parameter regimes adjacent to the chimera regime large-amplitude states invade the SAO regions, pushing out the decoherent SAOs there. Hence, the discovery that decoherent SAOs can coexist with coherent LAOs and MMOs is of substantial scientific interest.

Along with the minimal chimeras observed in a pair

^{a)}tasso@math.bu.edu

^{b)}theodore.vo@monash.edu

of symmetrically-coupled Langyel-Epstein oscillators²⁷, these mixed-amplitude chimeras are the first observations of chimeras in which the structures, amplitudes, and frequencies of the oscillations differ by orders of magnitude in the decoherent and coherent regions.

In addition, the new chimeras will be important for applications. Many bistable systems robustly exhibit SAOs, LAOs, and MMOs. See for example Refs. 30–49. Among these, models of various brain rhythms, cardiac rhythms, chemical waves, cell cycle transitions, and cell signaling with positive-feedback loops^{44–49}, share structural features of the model here. In particular, it is shown here that a pair of folded singularities, known as folded nodes and folded saddles, which arise in systems exhibiting MMOs, are important mechanisms responsible for creating the mixed-amplitude chimeras.

Also, a prominent application for which chimeras have been suggested as suitable models is unihemispheric slow-wave sleep (USWS)^{2,50–53}. In certain aquatic mammals and birds, one cerebral hemisphere sleeps and the other remains awake^{54,55}. This is illustrated by EEG recordings from bottlenose dolphins during USWS⁵⁴, in which one hemisphere exhibits synchronous high-amplitude, low-frequency oscillations characteristic of sleep⁵⁶, whilst the other shows desynchronized low-amplitude, high-frequency oscillations characteristic of wakefulness. We find here that the main properties of mixed-amplitude chimeras, with co-existing regions of coherent LAOs and MMOs and regions of decoherent SAOs are similar, at least in broad strokes. Of course, this is still far from establishing a possible role for mixed-amplitude chimeras in USWS. Instead, the existence of mixed-amplitude chimeras at least demonstrates that chimeras are relevant when the amplitudes and frequencies of the coherent and decoherent oscillations are widely different, something that has not been accounted for by the existing examples and theory of chimeras. Moreover, the mechanisms responsible for creating the mixed-amplitude chimeras (namely, the folded singularities of bistable systems) can be robust to small heterogeneities.

This article is organized as follows. In Section II, we study the prototypical bistable PDE with spatially-homogeneous reaction terms and purely local, isotropic diffusion, on which the mixed-amplitude chimeras were discovered. Also, we present the main dynamical properties and bifurcations of these chimeras. In Section III, we analyze the folded singularities which are the mechanisms responsible for allowing the identical oscillators to exhibit both the decoherent SAOs and the coherent MMOs, *i.e.*, the mechanisms responsible for the creation of the mixed-amplitude chimeras. In Section IV, the regions of SAO dynamics are examined in more detail, and it is reported that the recently-discovered phenomenon of delayed Hopf bifurcations plays an important role. In Section V, we study the bifurcation of these chimeras to a new type of pattern which consists of co-existing regions of coherent MMOs and coherent SAOs. Conclusions and discussion are presented in Section VI. Finally,

Section VII contains some open questions.

II. MIXED-AMPLITUDE CHIMERAS IN A PROTOTYPICAL BISTABLE PDE

The new mixed-amplitude chimera states are presented for a canonical multi-scale bistable PDE: the forced van der Pol equation with local diffusion^{38,57–66},

$$\begin{aligned} u_t &= v - u^2 - \frac{1}{3}u^3 + D_u u_{xx} \\ v_t &= \varepsilon(a - u + b \cos \theta) + D_v v_{xx} \\ \theta_t &= \varepsilon \omega. \end{aligned} \quad (1)$$

The activator (or voltage) u is fast, with bistable nullcline⁶⁷. The inhibitor (or recovery) v is slow, and $0 < \varepsilon \ll 1$ measures the scale separation in the reaction terms, as is common in bistable systems. The excitation threshold a , forcing amplitude b , frequency ω , and diffusivities D_u and D_v are spatially homogeneous, so that the kinetics and diffusion are identical and purely local at each point $x \in [0, 1]$. The boundary conditions are zero flux. Also, $\omega = 1$ unless stated otherwise so that the forcing period is $T = \frac{2\pi}{\varepsilon}$. The numerical methods and typical choices of initial data are described in the Appendix.

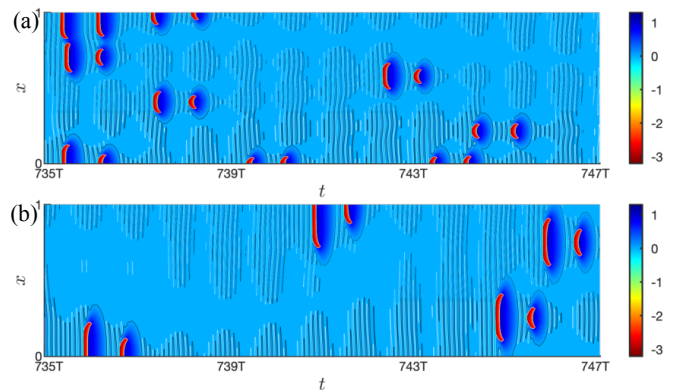


FIG. 1. Mixed-amplitude chimeras of (1). Coherent MMOs (red regions, followed by navy blue shadows) occur at random points and random times. All of the other regions exhibit decoherent SAOs (medium blue). Here, $a = -0.001$, $b = 0.005$, $\varepsilon = 0.01$. (a) $(D_u, D_v) = (0.45, 4) \cdot (\Delta x)^2$, (b) $(D_u, D_v) = (1.1, 11) \cdot (\Delta x)^2$. Contour lines at $u = \pm 2.5\sqrt{\varepsilon}$.

The mixed-amplitude chimeras of (1) exhibit coexisting regions of decoherent SAOs and coherent MMOs. The SAOs are classical phase waves about the depolarized state ($u = 0$). Diffusion decoheres them. The MMOs consist of coherent LAOs between the hyperpolarized state (near $u = -3$) and depolarized state, alternating with coherent SAOs. The MMOs occur either at random points and times (Fig. 1) or at fixed locations and time-periodically (Fig. 2), depending on (D_u, D_v) .

These mixed-amplitude chimeras are breathing, turbulent chimeras in the classification scheme presented in

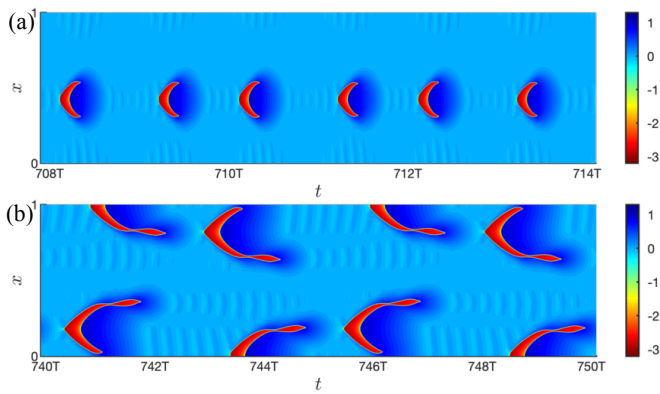


FIG. 2. Mixed-amplitude chimeras of breathing, turbulent type. (a) A fixed central band of coherent $2T$ -periodic MMOs, and decoherent SAOs in the complementary regions. $(D_u, D_v) = (1.4, 9) \cdot (\Delta x)^2$. Kinetics parameters as in Fig. 1. (b) Coherent $5T$ -periodic MMOs, and decoherent SAOs centrally. $(D_u, D_v) = (1.7, 9) \cdot (\Delta x)^2$ and $b = 0.002$.

Ref. 20. The spatial correlation $g_0(t) = \int_0^\delta g(|\hat{D}|, t) d|\hat{D}|$ was measured. Here, g is the normalized probability density of $|\hat{D}|$, where $\hat{D} = (\Delta x)^2 D$ is the scaled discrete Laplacian, $\delta = 0.01 D_m$ is the threshold below which the profile is regarded as coherent, and D_m is the absolute maximal curvature. For (1), $g_0(t)$ exhibits a pair of fast jumps (one up and one down) for each spatially coherent MMO. See Fig. 3(a). Moreover, these pairs of fast jumps occur at random times for the chimeras in Fig. 1 and time-periodically for those in Fig. 2 (see Fig. 3(a)). Moreover, between jumps, $g_0(t)$ fluctuates randomly, due to the decoherent SAOs, remaining well inside the interval $(0, 1)$. Hence, the solution is a breathing, turbulent chimera.

The temporal correlation $h_0 = \sqrt{\int_\gamma^1 h(|\rho|) d|\rho|}$ of Ref. 20 was also measured. Here, ρ_{ij} is the correlation coefficient for the time series at x_i and x_j , and h is the probability distribution function of $|\rho|$. We find that, over large times, h_0 converges to zero when the MMO clusters occur randomly. This is consistent with the observations that the positions of the coherent clusters change in time. In contrast, for the chimeras in which the coherent MMO clusters are fixed in space, we find that h_0 is a non-zero constant inside $(0, 1)$. See Fig. 3(a).

The mixed-amplitude chimeras of (1) are observed robustly where D_u is sufficiently less than D_v ; see Fig. 4. The typical chimeras (marked by red circles) have coherent MMOs which occur at random points and at random times, with decoherent SAOs in all other regions, just like the chimeras shown in Fig. 1. There are also wedges in the $D_u - D_v$ parameter space in which the chimeras have coherent MMOs that are time-periodic and spatially fixed (blue circles), examples of which are given by the chimeras shown in Fig. 2. Moreover, in all of these chimeras, the decoherent SAOs occupy an increasing portion of $[0, 1]$ as D_u decreases, within this regime.

At the right edge of the mixed-amplitude chimeras

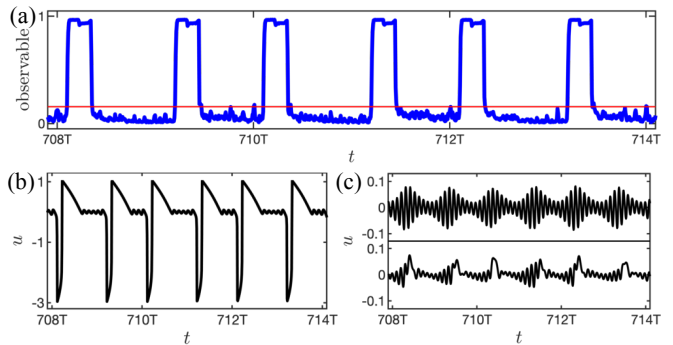


FIG. 3. (a) Coherence measures $g_0(t)$ (blue) and h_0 (red) of the chimera in Fig. 2(a). Time series of u in the (b) coherent MMO region ($x = 0.45$), (c) decoherent SAO domain ($x = 0.1, 0.21$). The amplitudes and frequencies differ significantly.

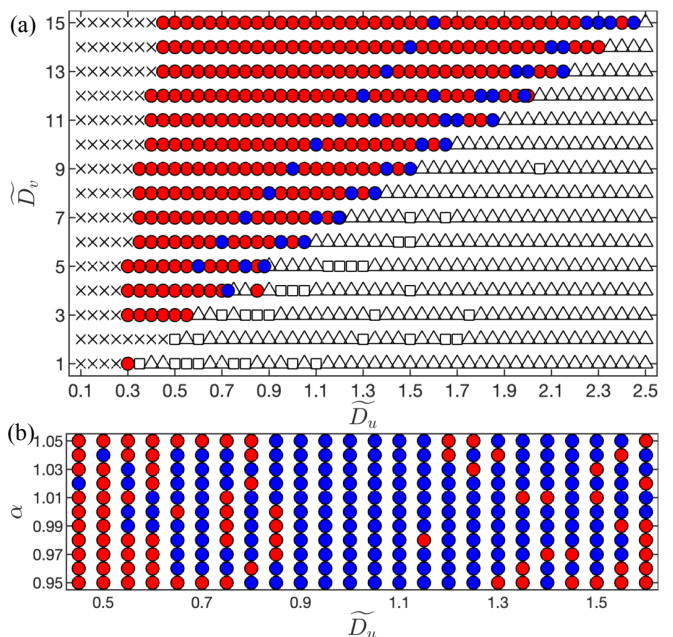


FIG. 4. Mixed-amplitude chimeras exist for $D_u < D_v$ ($D_i = \tilde{D}_i (\Delta x)^2$, $i = u, v$). (a) ● Breathing turbulent chimeras with randomly-occurring coherent MMOs. ● Breathing chimeras with time-periodic, spatially-fixed coherent MMOs. × Sharp interface solutions. △ Spatially uniform, time-periodic MMOs. □ Trigger waves exhibiting time-periodic annihilation and nucleation of MMOs. Kinetics as in Fig. 1 (b) In the strip $\tilde{D}_v = (1/\sqrt{\varepsilon})\tilde{D}_u - 1 = 10\tilde{D}_u - \alpha$, for $\alpha \in [0.95, 1.05]$, many chimeras have time-periodic MMOs. For each set of parameters, (1) was integrated for a total time of $750T$.

regime in Fig. 4, the chimeras bifurcate to spatially-uniform, time-periodic MMOs (Fig. 5(a)) and to trigger waves (Fig. 5(b))⁶⁸. Here, D_u is no longer small enough relative to D_v . The SAO regions are displaced (in part or entirely) by MMOs and trigger waves. The trigger wave patterns, such as in Fig. 5(b), can exhibit annihilation points where pairs of traveling waves of MMOs moving

in opposite directions collide and eliminate each other in the interior of the spatial domain. This annihilation event is typically followed some time later by a nucleation point at the same spatial location where a pair a trigger waves emerge and radiate away from the nucleation point in opposite directions.

Further, we observe that the presence of the spatially coherent MMOs and trigger waves in this parameter regime immediately adjacent to the regime of mixed-amplitude chimeras makes the existence of these chimeras all the more striking. In mixed-amplitude chimeras, the decoherent SAOs resist the invasion of the stable LAO/MMOs.

At the left edge of the mixed-amplitude chimera regime in Fig. 4, the chimeras bifurcate from sharp-interface solutions³⁷. As shown in Fig. 5(c), these sharp interface solutions have steep jumps at fixed locations connecting the depolarized and hyperpolarized states. Then, on the spatial intervals between the jumps, these solutions exhibit time-periodic SAOs.

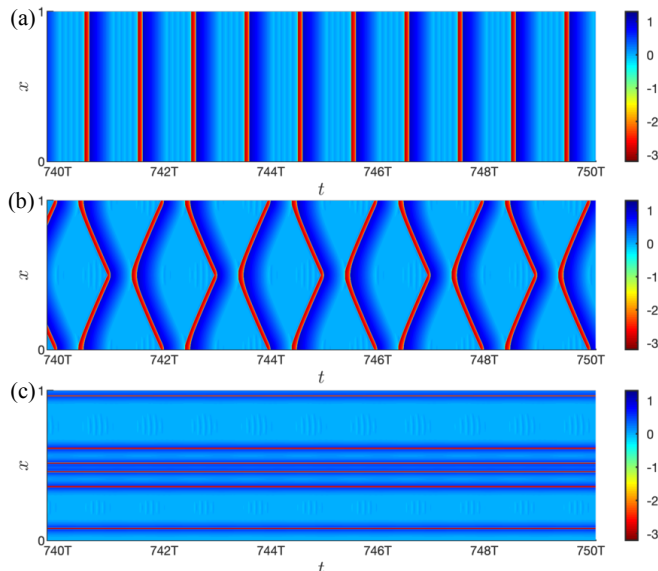


FIG. 5. (a) A representative spatially homogeneous, T -periodic MMO state of (1) of the type denoted by Δ in Fig. 4. Here, $\widetilde{D}_u = 1$ and $\widetilde{D}_v = 5$. (b) A representative trigger wave exhibiting time-periodic annihilation and nucleation of MMOs, of the type denoted by \square in Fig. 4. Here, $\widetilde{D}_u = 1.7$ and $\widetilde{D}_v = 7$. (c) A representative sharp-interface solution of the type denoted by \times in Fig. 4. Here, $\widetilde{D}_u = 0.15$ and $\widetilde{D}_v = 3$.

Overall, as shown in Fig. 4, it is also a novelty of mixed-amplitude chimeras that they bifurcate from large-amplitude solutions, which are ubiquitous in bistable systems, and not from homogeneous or drift states.

Mixed-amplitude chimeras also exhibit multi-stability and symmetry-breaking. For example, the chimera state in Fig. 2(a) coexists with three other stable states of (1) for the same parameters. There is a co-existent spatially-homogeneous SAO state. Also, there are two

other mixed-amplitude chimeras, one of which resembles the reverse image, with coherent MMOs along the boundaries and a central strip of decoherent SAOs, and the other of which has time-periodic coherent MMOs both in the central region, as the chimera in Fig. 2(a), and near the boundaries, as well as decoherent SAOs everywhere else. Furthermore, symmetry-breaking occurs through bifurcations to chimeras in which the widths of the MMO regions vary time-periodically.

III. FOLDED SINGULARITIES AS A MECHANISM FOR MIXED-AMPLITUDE CHIMERAS

A distinct mechanism, structurally different from that in known chimeras, is at the heart of the mixed-amplitude chimeras. There is a pair of commonly-occurring singularities, known as folded nodes (FNs) and folded saddles (FSs), in the kinetics of bistable PDEs. These singularities arise naturally in the van der Pol oscillator (1)^{62–64}, and in neuroscience, physics, chemistry, and electrical engineering models^{27,31–33,65,69–76}.

The FN and FSs lie on a fold curve between attracting and repelling sheets of the slow manifold. For (1), they are located at the points $\theta_{N,S}$ where $a + b \cos(\theta_{N,S}) = 0$, for all $0 < |a| < b$, as may be calculated from the ODE consisting of the reaction terms in (1), see Refs. 64 and 77. See Fig. 6.

In the decoherent regions, the time traces of the SAOs are observed to pass through neighbourhoods of FN and FSs in alternation, Fig. 6(a,b). Near a FN, the SAOs are centred on its weak canard^{65,76}. As the time traces approach the next FS, the SAOs are centred about its faux canard⁷⁰. The weak and faux canards (approximated by the green curves) lie $\mathcal{O}(b)$ -close to the fold curve, as expected from the ODE⁶³. In the passage from an FN to an FS and then through a neighbourhood of the FS, the amplitude grows until there is an excursion (near the repelling branch of the slow manifold), into the funnel region (gray) of the next FN. Hence, the time trace enters the neighbourhood of the next FN, since the funnels are basins of attraction for the FN³³, and there it has further SAOs about the weak canard of that FN.

In the coherent region(s), the time traces are seen to be MMOs induced by the canards of the folded singularities^{31–33,69} (Fig. 6(c,d)). The SAO segments of these MMOs are also about the FN weak canard. However, here, after passage near a FN, there is a large-amplitude excursion toward the lower attracting sheet of the slow manifold. Subsequently, the traces crawl along this sheet until they reach the lower fold curve, where they jump back to the upper sheet and into the funnel of the next FN, and the cycle repeats. (The funnel is enclosed by the true canard (magenta) of the FS^{70,73}, the strong canard (cyan) of the FN^{33,76}, and the fold curve.) These MMOs remain spatially coherent in the presence of diffusion, due to the LAOs.

Overall, we find that there is a robust zone –which we

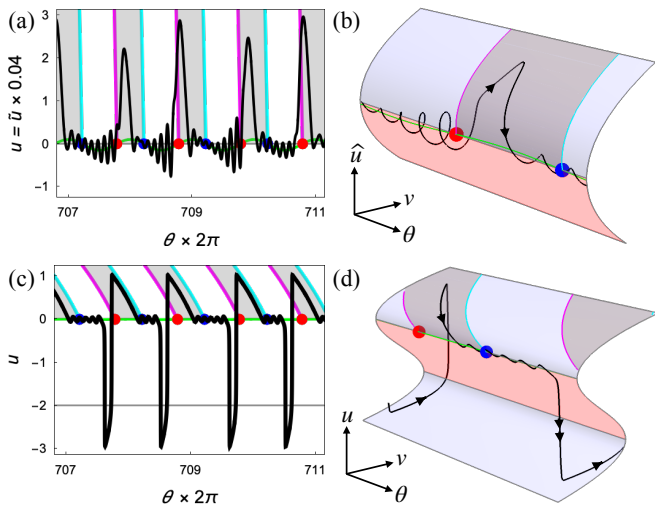


FIG. 6. Time traces (black) of the chimera in Fig. 2, at $x = 0.23$ in (a) and (b), and at $x = 0.41$ in (c) and (d). In the decoherent SAO regions, the time traces oscillate about the weak canards of the FNs (blue dots) and the faux canards of the FSs (red dots), near the attracting (upper) sheet and repelling (middle) sheet of the slow manifold. In the coherent MMO regions, the time traces also have LAOs down to the lower branch of the attracting slow manifold.

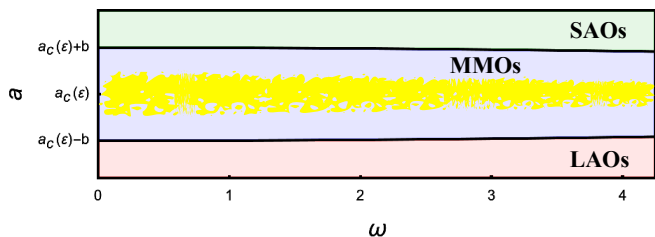


FIG. 7. Mixed-amplitude chimeras of (1) are robust in the goldilocks zone (gold) of the (ω, a) plane. It sits in the middle of the MMO region, which is enclosed by $a = a_c(\epsilon) \pm b e^{-\epsilon\omega^2/2}$, *i.e.*, by the saddle-node bifurcations of the FN and FS canards⁶⁴. For the classical van der Pol equation, $a_c(\epsilon) = -\frac{\epsilon}{8} - \frac{3\epsilon^2}{32} + \mathcal{O}(\epsilon^3)$ ⁷⁸.

label as a goldilocks zone— in which the mixed-amplitude chimera states exist in (1). See Fig. 7. In this goldilocks zone, the distances between the FNs and FSs are simultaneously small and large enough. The distances are small enough that, on wide intervals, the attractor of (1) can pass near the FNs and FSs in alternation, with the amplitude remaining small and diffusion causing the decoherence. They are also large enough that, in complementary MMO regions, the return mechanisms for the LAO segments are robust.

The goldilocks zone shown in Fig. 7 is representative of the zones in the (ω, a) plane for a range of values of b . Hence, mixed-amplitude chimeras are robust in (1).

IV. DELAYED HOPF BIFURCATIONS UNDERLIE THE DECOHERENT SAOS

Having presented the novel mixed-amplitude chimeras, the parameter regime in which they exist, the bifurcations in which they are created or annihilated, and the folded nodes and folded saddles which make it possible for these identical oscillators to exhibit both SAO and LAO/MMO dynamics, we next turn to a fundamental question about the SAO dynamics. Namely, what is the mechanism by which the solutions in the decoherent regions can remain close to the fold curve long enough so that they can pass through the neighbourhoods of both the FN and the FS, hence keeping the oscillation amplitudes small? This question is important, since it is expected that solutions which pass through a neighbourhood of a FN generally are repelled away from the fold curve and rapidly approach the (hyperpolarized) attracting branch of the slow manifold, resulting in large-amplitudes. It turns out, as we show here, that the SAOs in the decoherent regions can exist due to delayed passage through Hopf bifurcations (DHB). That is, DHB makes it possible for large measures of solutions to stay near the fold curve (and hence maintain small amplitude) so that they not only pass through a neighbourhood of the FN, but also stay close enough to pass through a neighbourhood of the FS and into the funnel of the next FN, so that the cycle can repeat.

To show this, we study (1) with parameters chosen so that the FN and the FS are close to $\theta = 0 \pmod{2\pi}$. This includes the parameters in the goldilocks zone.

First, we show that the local dynamics of (1) may be studied using two coupled CGL-type equations with a slowly-varying parameter. In particular, we rescale $u = \sqrt{\epsilon}u_2$, $v = \epsilon v_2$, $\theta = \epsilon^{1/4}\theta_2$, $\tau = \sqrt{\epsilon}t$, $a + b = \sqrt{\epsilon}\alpha_2$, and $D_i = \sqrt{\epsilon}d_i$ ($i = u, v$), so (1) becomes

$$\begin{aligned} u_{2\tau} &= v_2 - u_2^2 - \frac{1}{3}\sqrt{\epsilon}u_2^3 + d_u u_{2xx} \\ v_{2\tau} &= -u_2 + \alpha_2 - \frac{1}{2}b\theta_2^2 + \mathcal{O}(\sqrt{\epsilon}\theta_2^4) + d_v v_{2xx} \\ \theta_{2\tau} &= \epsilon^{1/4}\omega. \end{aligned}$$

This rescaling focuses on the dynamics in the neighborhood of a FN-FS pair. This local model consists of a fast-slow system, with (u_2, v_2) as the fast variables and θ_2 as the slow variable.

We rectify the critical manifold to the θ_2 -axis using $\tilde{u}_2 = u_2 + \mu$ and $\tilde{v}_2 = v_2 - \mu^2$, where $\mu = -\alpha_2 + \frac{b}{2}\theta_2^2$. Also, we switch to the complex coordinates $z = \tilde{u}_2 + i\tilde{v}_2$ and $\bar{z} = \tilde{u}_2 - i\tilde{v}_2$, which are more natural variables for studying the slow passage through a Hopf bifurcation. Hence, (1) is locally equivalent to

$$\begin{aligned} \begin{bmatrix} z \\ \bar{z} \end{bmatrix}_\tau &= \begin{bmatrix} \mu - i & \mu \\ \mu & \mu + i \end{bmatrix} \begin{bmatrix} z \\ \bar{z} \end{bmatrix} - Q \begin{bmatrix} 1 \\ 1 \end{bmatrix} + \begin{bmatrix} d_+ & d_- \\ d_- & d_+ \end{bmatrix} \begin{bmatrix} z \\ \bar{z} \end{bmatrix}_{xx} \\ \mu_\tau &= \epsilon^{1/4}\omega\sqrt{2b(\mu + \alpha_2)}, \end{aligned}$$

where $Q = \frac{1}{4}(z + \bar{z})^2$ and $d_\pm = \frac{1}{2}(d_u \pm d_v)$. The origin

is an attracting spiral of the (z, \bar{z}) system for each $\mu < 0$ and a repeller for each $\mu > 0$.

Due to the slow growth in μ , this PDE exhibits a dynamic Hopf bifurcation at $\mu = 0$. In particular, solutions initialised with $\mu < 0$ do not immediately diverge from the equilibrium when μ crosses zero and becomes positive. Instead, they remain near the repelling state for long times beyond the dynamic Hopf point (data not shown), in a delayed Hopf bifurcation (DHB). The time of the delay, past $\mu = 0$, is $\mathcal{O}(1)$ in the slow time, so that solutions spend long times near the repelling sheet of the slow manifold in the robust SAO regions. Moreover, these times are long enough so that the solutions can pass near a pair of FN and FS and reach the basin of attraction (funnel) of the next FN, keeping the oscillation amplitude small.

Remark. For this system of coupled CGL-type PDEs, the observed DHB is consistent with the recent discovery of DHB in nonlinear PDEs^{79,80}, including the Hodgkin-Huxley PDE, Brusselator model, and CGL equation. See also Ref. 81.

Remark. The analysis here of DHB in these PDEs was inspired by the ODE analysis in Ref. 63. There, singularities known as Folded Saddle Nodes of Type 1 (FSN I), which arise in bifurcations of FNs and FSs, are studied in ODEs. The analysis in Ref. 63 shows that delayed Hopf bifurcation plays a central role in ODEs near FSN I bifurcations. Hence, it was natural here to examine the regime in which the FN and FS of (1) are close together, and to look for DHB also in the PDE (1).

V. BIFURCATION TO COHERENT-COHERENT STATES

The above analyses of the folded singularities (Sec. III) and of the scaling leading to the coupled CGL-type model for the local dynamics (Sec. IV) also apply for larger b (relative to ε), outside the main chimera regime. With stronger forcing (larger b), the attractors also consist of regions with coherent MMOs and complementary regions of SAOs. However, we find that with larger b the pure-SAO states are coherent in the presence of diffusion, rather than decoherent as in the mixed-amplitude chimeras. These coherent-coherent patterns are multi-mode attractors in the sense of Ref. 82.

Examples of these multi-mode attractors, which feature coherent MMOs and coherent SAOs are shown in Fig. 8. Some of these have multiple sharp interfaces separating the regions, and others do not have any sharp interfaces. For example, in Fig. 8(b), one finds an attractor of (1) with three distinct types of regions: a region of coherent MMOs, a region in which the time traces are near the hyperpolarized state (near $u = -3$), and a region of coherent SAOs about the depolarized state. With the knowledge of the FNs and FSs, one can construct rich patterns.

Furthermore, in these coherent-coherent states that exist for larger b , the time traces of the attractor also exhibit maximal spatiotemporal canards in the transition intervals between the two distinct states (as for example near the bulbs in Fig. 8(c)). These maximal spatiotemporal canards mediate the transitions between regions of distinct oscillatory behaviour, similar to those in Ref. 82.

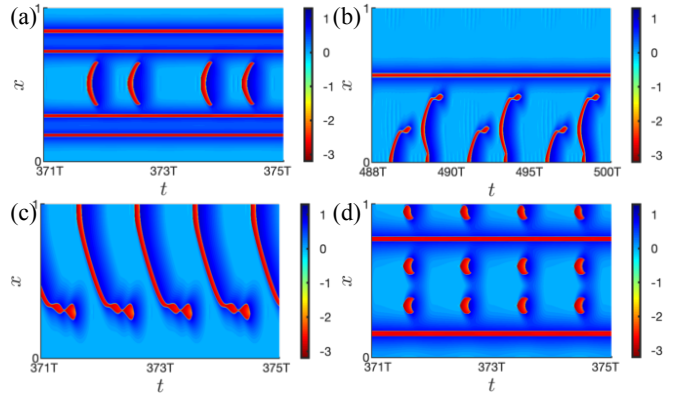


FIG. 8. A sample of coherent-coherent multi-mode attractors for various ratios of ε to b . (a) $\varepsilon = b = 0.005$ with $(D_u, D_v) = (0.47, 4) \cdot (\Delta x)^2$. (b) $\varepsilon = b = 0.01$ with $(D_u, D_v) = (1.71, 9) \cdot (\Delta x)^2$. (c) $\varepsilon = \frac{1}{2}b = 0.005$ with $(D_u, D_v) = (1.40625, 11.25) \cdot (\Delta x)^2$. (d) $\varepsilon = \frac{1}{5}b = 0.005$ with $(D_u, D_v) = (0.325, 8) \cdot (\Delta x)^2$. Finally, for each fixed pair of ε and b , the kinetics parameter a is chosen to lie in the goldilocks zone: (a) $a = -0.001$, (b) $a = -0.001$, (c) $a = -\frac{\varepsilon}{8} + \frac{1}{10}be^{-\varepsilon\omega^2/2} \approx 0.000372503$ and (d) $a = -\frac{\varepsilon}{8} + \frac{1}{20}be^{-\varepsilon\omega^2/2} \approx 0.000621879$.

VI. CONCLUSIONS AND DISCUSSION

In this article, we presented the novel class of chimeras labeled as mixed-amplitude chimeras, which consist of co-existing decoherent SAOs and coherent LAOs or MMOs. This constitutes the first observation of chimeras in PDEs in which the structures, amplitudes, and frequencies of the oscillations are widely separated in the two distinct types of regions. With the exception of Ref. 27, these chimeras differ from the known chimeras and theory, where the amplitudes and frequencies in the coherent and decoherent regions are comparable.

These mixed-amplitude chimeras are surprising, since the coherent LAOs and MMOs have much larger amplitudes and since they are structurally stable. Moreover, in parameter regimes immediately adjacent to the chimera regime, the LAOs and MMOs are observed to invade the decoherent regions and wipe out the SAOs. Indeed, new bifurcations were also discovered in which mixed-amplitude chimeras emerge from spatially-uniform MMOs, trigger waves, and sharp-interface solutions, all of which are ubiquitous in bistable PDEs.

Initial theory has been identified for the mixed-amplitude chimeras. It was shown here that they are

generated by folded node and folded saddle singularities, common in bistable systems. Moreover, it was discovered that there is a robust goldilocks zone in which the mixed-amplitude chimeras exist, where the inter-singularity distances are simultaneously small and large enough so the decoherent SAOs and coherent MMOs can co-exist. Also, it was shown that Delayed Hopf Bifurcations in PDEs enables the existence of the SAOs in the decoherent regions.

The mixed-amplitude chimeras may have important applications in bistable systems, which are often used to model biological, chemical, and physical rhythms.

The mixed-amplitude chimeras also bear some of the hallmarks of EEG recordings taken from animals that exhibit USWS⁵⁴. Namely, the regions of coherent MMOs consist of large-amplitude, low-frequency activity as observed in the sleeping hemisphere, and the regions of decoherent SAOs consist of small-amplitude, high-frequency activity similar to the awake hemisphere.

The substantial contrasts in amplitudes and frequencies observed here for the mixed-amplitude chimeras of (1) are similar in some respects to the contrasts reported recently in minimal chimeras in Ref. 27. There, a two-cell model consisting of a pair of symmetrically-coupled Lengyel-Epstein ODEs is studied. The parameters are tuned near a canard point of the L-E system, with one oscillator exhibiting periodic LAOs and the other aperiodic SAOs. Moreover, the existence of new types of phase relations between coupled cells was established, distinct from the classical in-phase and anti-phase attractors in coupled fast-slow systems. Using analysis similar to that presented in this article, it can be shown that the underlying singularity in Ref. 27 is a (type III) folded saddle-node, and the parameters are in its goldilocks zone.

The mixed-amplitude chimeras introduced here are distinct from the Multi-Mode Attractors presented in Ref. 82. There, the MMAs were introduced in systems with spatially-dependent parameters. The spatially-dependent applied currents (or spatially-dependent maximal ion-channel conductivities) give rise to attractors that exhibit different modes of oscillations in different spatial regions. Hence, in the systems with MMAs, the oscillators are not all identical. In contrast, here, the reactions are all spatially homogeneous and the diffusion is purely local and isotropic, so that the oscillators at each point are identical. See also the discussion in the introductory section 1 of Ref. 82.

VII. SOME OPEN QUESTIONS

The discovery of mixed-amplitude chimeras raises a number of questions. First, it is of interest to investigate the mechanism(s) by which some of the mixed-amplitude chimeras can have coherent MMOs that occur at fixed locations in space and periodically in time. These are indicated by the blue circles in the $D_u - D_v$ parameter plane in Fig. 4. As discussed above, these are distinct from the typical chimeras (red circles), in which the co-

herent MMOs occur at random points and at random times. There may be some type of resonance responsible for creating these wedges of blue circles within the sea of red circles.

Second, we ask if some of the known examples of chimeras in other systems can be continued to parameter regimes in which the structures, amplitudes, and/or frequencies of the coherent oscillations are substantially different from those of the decoherent SAOs, as is the case for the mixed-amplitude chimeras here. The known examples and theory of chimera states in coupled oscillators, integro-differential systems, and PDEs are based on the amplitude-phase method or mean-field approach^{1,2,14,18,24}, symmetry and broken symmetry analyses^{16,23}, and the theory^{4,29} of desynchronization-induced stabilization of coherent oscillations, among other important results. These methods have been used primarily to find chimeras in which the amplitudes and frequencies of the oscillations in the decoherent and coherent regions are comparable, *i.e.*, where they do not differ by orders of magnitude. For example, the analysis used in the phase-amplitude method is premised on the fact that the oscillations in the chimera states and the states from which bifurcate have similar amplitudes and frequencies. Hence, it would be of interest to explore whether any of these may be continued in parameter space so that the coherent regions exhibit LAOs and MMOs.

In the other direction, one may ask whether the new mixed-amplitude chimeras can be continued in parameter space to a regime in which the coherent oscillations are near homogeneous states (and hence purely of SAO type), instead of being MMOs or LAOs.

Third, there is a natural question about what the minimal dimension is for a system to exhibit mixed-amplitude chimeras. We recall that, in ODEs, three is the minimum number of variables necessary for MMOs. This is the case for the forced van der Pol reaction terms in (1). It is also the case for the Lengyel-Epstein ODEs studied in Ref. 27, where an individual L-E model has two dependent variables, and the systems studied there consist of two symmetrically-coupled L-E oscillators (*i.e.*, four variables), or of a single L-E oscillator with some type of external forcing (*i.e.*, three variables). Hence, the results of Ref. 27 and this article suggest that three variables in the kinetics is expected to be the minimum number needed for chimera states to exhibit co-existing regions of coherent MMOs and decoherent SAOs, such as the mixed-amplitude chimeras reported here.

ACKNOWLEDGMENTS

The authors thank Karen Corbett for useful conversations and support with MASSIVE. We also thank Irv Epstein, Ryan Goh, Christian Kuehn, Jonathan Touboul, Gene Wayne, and Martin Wechselberger for useful comments and questions. The research of T.V. was par-

tially supported by NSF-DMS 1853342. The research of T.K. was partially supported by NSF-DMS 1616064. This work was supported by the MASSIVE HPC facility (www.massive.org.au).

VIII. APPENDIX

The numerical simulations were performed using the method of lines, with adaptive time-stepping suited to stiff problems, and a second-order spatial discretization. The results were confirmed independently using four other methods: balanced symmetric Strang operator splitting, with (second-order) centered finite differences in space and fourth-order Runge-Kutta in time; the Crank-Nicholson method, which is second-order accurate in both space and time; a compact finite difference method which is fourth-order accurate in space; and, a Chebyshev grid method that is spectral in space. All simulations were run at least for the order of the diffusive time scale, based on the smaller diffusivity. Unless stated otherwise, $N_x = 750$ spatial subintervals were used ($\Delta x = \frac{1}{750}$). Also, convergence was checked with smaller values of Δx .

The main method used to generate initial data ($u_0(x), v_0(x)$) on $[0, 1]$ is to compute a limit cycle attractor ($\Gamma_u(t), \Gamma_v(t)$) (period T) of the kinetics ODE, and then to set $(u_0(x), v_0(x)) = (\Gamma_u(\frac{t}{nT}), \Gamma_v(\frac{t}{nT}))$. Typical initial data consists of n copies spread out in space, with $\theta(t=0) = 0$. For example, $n = 6$ in Fig. 4. Eight other types of initial data were also used to explore more fully the multi-stable landscape of solutions, and to find chimera states.

- ¹Y. Kuramoto and D. Battogtokh, *Nonlin. Phen. Complex Sys.* **5**, 380 (2002). Y. Kuramoto, in *Nonlin. Dyn. Chaos: Where Do We Go from Here?*, S.J. Hogan, A.R. Champneys, B. Krauskopf, M. di Bernardo, H.M. Osinga, and M.E. Homer (eds.), IOP, Bristol, UK, 209 (2003). Y. Kuramoto and S.I. Shima, *Prog. Theor. Phys. Suppl.* **150**, 115 (2003). S.I. Shima and Y. Kuramoto, *Phys. Rev. E* **69**, 036213 (2004).
- ²D.M. Abrams and S.H. Strogatz, *Phys. Rev. Lett.* **93**, 174102 (2004). D.M. Abrams, R.E. Mirollo, S.H. Strogatz, D.A. Wiley, *Phys. Rev. Lett.* **101**, 084103 (2008).
- ³E. Ott and T.M. Antonsen, *Chaos* **18**, 037113 (2008). E. Ott and T.M. Antonsen, *Chaos* **19**, 023117 (2009).
- ⁴O.E. Omel'chenko, Y.L. Maistrenko, and P.A. Tass, *Phys. Rev. Lett.* **100**, 044105 (2008).
- ⁵G. Bordyugov, A. Pikovsky, and M. Rosenblum, *Phys. Rev. E* **82**, 035205(R) (2010).
- ⁶C. Laing, *Phys. Rev. E* **81**, 066221 (2010).
- ⁷C. Laing, *Phys. Rev. E* **92**, 050904(R) (2015). C. Laing, *Phys. Rev. E* **100**, 042211 (2019).
- ⁸I. Omelchenko, Y. Maistrenko, P. Hövel, and E. Schöll, *Phys. Rev. Lett.* **106**, 234102 (2011). I. Omelchenko, O. E. Omel'chenko, P. Hövel, and E. Schöll, *Phys. Rev. Lett.* **110**, 224101 (2013).
- ⁹M.R. Tinsley, S. Nkomo, and K. Showalter, *Nature Phys.* **8**, 662 (2012).
- ¹⁰A.M. Hagerstrom, T. E. Murphy, R. Roy, I. Omelchenko, P. Hövel, and E. Schöll, *Nature Phys.* **8**, 658 (2012).
- ¹¹E.A. Martens, S. Thutupalli, A. Fourriere, and O. Hallatschek, *PNAS* **110**, 10563 (2013).
- ¹²S. Nkomo, M.R. Tinsley, and K. Showalter, *Phys. Rev. Lett.* **110**, 244102 (2013).
- ¹³K. Schönleber, C. Zensen, A. Heinrich, and K. Krischer, *New J. Phys.* **16**, 063024 (2014). L. Schmidt, K. Schönleber, K. Krischer, and V. Garcia-Morales, *Chaos* **24**, 013102 (2014). L. Schmidt and K. Krischer, *Chaos* **25**, 064401 (2015).
- ¹⁴G.C. Sethia and A. Sen, *Phys. Rev. Lett.* **112**, 144101 (2014).
- ¹⁵A. Yeldesbay, A. Pikovsky, and M. Rosenblum, *Phys. Rev. Lett.* **112**, 144103 (2014).
- ¹⁶A. Zakharova, M. Kapeller, and E. Schöll, *Phys. Rev. Lett.* **112**, 154101 (2014).
- ¹⁷I. Omelchenko, A. Provata, J. Hizanidis, E. Schöll, and P. Hövel, *Phys. Rev. E* **91**, 022917b (2015).
- ¹⁸M.J. Panaggio and D.M. Abrams, *Nonlinearity* **28**, R67 (2015).
- ¹⁹M.G. Clerc, S. Coulibaly, M.A. Ferre, M.A. Garcia-Nustes, and R.G. Rojas, *Phys. Rev. E* **93**, 052204 (2018).
- ²⁰F. P. Kemeth, S. W. Haugland, L. Schmidt, I. G. Kevrekidis, and K. Krischer, *Chaos* **26**, 094815 (2016).
- ²¹B.-W. Li and H. Dierckx, *Phys. Rev. E* **93**, 020202(R) (2016). B.-W. Li, Y. He, L.-D. Li, L. Yang, X. Wang, *Arxiv* 2012.00983, nlin, Dec 2020.
- ²²Z.G. Nicolau, H. Riecke, and A.E. Motter, *Phys. Rev. Lett.* **119**, 244101 (2017).
- ²³F.P. Kemeth, S.W. Haugland, and K. Krischer, *Phys. Rev. Lett.* **120**, 214101 (2018).
- ²⁴O.E. Omel'chenko, *Nonlinearity* **31**, R121 (2018).
- ²⁵J.F. Tetz, J. Rode, M.R. Tinsley, K. Showalter, and H. Engel, *Nat. Phys.* **14**, 282 (2018). J. Rode, J.F. Tetz, E. Fengler, and H. Engel, *Frontiers Appl. Math. Stat.* **5**, 31 (2019). J.F. Tetz, M.R. Tinsley, H. Engel, and K. Showalter, *Nat. Sci. Rep.* **10**, 7821 (2020).
- ²⁶S. Kundu, S. Majhi, P. Muruganandam, D. Ghosh, *Eur. Phys. J. Spec. Topics* **227**, 983–993 (2018).
- ²⁷N.M. Awal, D. Bullara, and I.R. Epstein, *Chaos* **29**, 013131 (2019). N.M. Awal and I.R. Epstein, *Phys. Rev. E* **101**, 042222 (2020).
- ²⁸I.A. Shepelev and V.S. Anischenko, *Comm. Nonlin. Sci., Num. Sim.* **93**, 105513 (2021).
- ²⁹Y. Zhang and A.E. Motter, *Phys. Rev. Lett.* **126**, 094101 (2021).
- ³⁰M. Brons, T.J. Kaper, and H.G. Rotstein, *Chaos* **18**, 015101 (2008).
- ³¹M. Desroches, J. Guckenheimer, B. Krauskopf, C. Kuehn, H.M. Osinga, and M. Wechselberger *SIAM Rev.* **54**, 211 (2012).
- ³²E. Harvey, V. Kirk, M. Wechselberger, and J. Sneyd, *J. Nonlin. Sci.*, **21** 639–683 (2011).
- ³³J.E. Rubin and M. Wechselberger, *Bio. Cybernetics* **97**, 5 (2007). M. Bröns, M. Krupa, and M. Wechselberger, *Fields Inst. Commun.* **49**, 39–63 (2006).
- ³⁴M. Koper, *Physica D* **80**, 72 (1995).
- ³⁵D. Walgraef, *Spatio-Temporal Pattern Formation*, Springer, New York (1997).
- ³⁶W. van Saarloos, *Phys. Rep.*, **386**, 29 (2003).
- ³⁷Y. Nishiura, *Far-from Equilibrium Dynamics*, Amer. Math. Soc., Transl. Math. Monographs, **209** (2002).
- ³⁸J. Keener and J. Sneyd, *Mathematical Physiology I: Cellular*

- Physiology*, 2nd ed., Springer, New York (2009).
- ³⁹A. Hodgkin and A. Huxley, *J. Physiol.* **117**, 500 (1952).
- ⁴⁰J. Moehlis, *J. Math. Bio.* **52**, 141 (2006).
- ⁴¹R. FitzHugh, *J. Gen. Physiol.* **43**, 867 (1960).
- ⁴²J. Nagumo, S. Arimoto, and S. Yoshizawa, *Proc. IRE* **50**, 2061 (1962).
- ⁴³R.R. Aliev and A.V. Panfilov, *Chaos Soliton Fract* **7**, 293 (1996).
- ⁴⁴D. Angeli, J.E. Ferrell, and E.D. Sontag, *PNAS*, **101**, 1822 (2004).
- ⁴⁵J. Rombouts and L. Gelens, *PLOS Comp. Bio.*, **17**, 1008231 (2021).
- ⁴⁶I. Lengyel, G. Rabai, and I.R. Epstein, *J. Am. Chem. Soc.* **112**, 9104 (1990). I. Lengyel and I.R. Epstein, *Science* **251**, 650 (1991).
- ⁴⁷I. Erchova and D.J. McGonigle, *Chaos* **18**, 015115 (2008).
- ⁴⁸C.G. Diniz Behn, E.N. Brown, T.E. Scammell, and N. Kopell, *J. Neurophysiol.* **97**, 3828-3840 (2007).
- ⁴⁹X.-J. Wang, *Physiol. Rev.* **90**, 1195-1268 (2010).
- ⁵⁰A.E. Motter, *Nat. Phys.* **6**, 164-165 (2010).
- ⁵¹L. Ramlow, J. Sawicki, A. Zakharova, J. Hlinka, J.C. Claussen, and E. Schöll, *EPL* **126**, 50007 (2019).
- ⁵²S.W. Haugland, L. Schmidt, and K. Krischer, *Sci. Rep.-UK* **91**, 40006 (2010).
- ⁵³R. Ma, J. Wang, and Z. Liu, *EPL* **91**, 40006 (2010).
- ⁵⁴N.C. Rattenborg, C.J. Amlaner, and S.L. Lima, *Neurosci. Behav. Rev.* **24**, 817-842 (2000).
- ⁵⁵N.C. Rattenborg, *Naturwissensch.* **93**, 413-425 (2006).
- ⁵⁶M. Steriade, D.A. McCormick, and T.J. Sejnowski, *Science* **262**, 679-685 (1993).
- ⁵⁷B. van der Pol, *Radio Review* **1**, 701 (1920). B. van der Pol, *Lond., Edinb., Dublin Phil. Mag. & J. Sci., Series 7*, **3**, 65-80 (1927).
- ⁵⁸A.B. Vasil'eva, S.A. Kashchenko, Yu.S. Kolesov, and N.Kh. Rozov, *Math. USSR Sbor.* **58**, 491 (1987).
- ⁵⁹K.R. Schneider and V.M. Evtukhov, *Differentsial'nye Urav.* **24**, 1027 (1988) (Eng. transl.: *Diff. Eq.* **24**, 683).
- ⁶⁰D. Kaplan and L. Glass, *Understanding Nonlinear Dynamics*, Springer, New York (1995).
- ⁶¹M.L. Fachinetti, E. de Langre, and F. Biolley *Comp. Rend. Acad. Sci., Paris, Ser. II* **330** (2002).
- ⁶²J. Guckenheimer, K. Hoffman, and W. Weckesser, *SIAM J. Appl. Dyn. Sys.* **2**, 1 (2003); K. Bold, C. Edwards, J. Guckenheimer, S. Guharay, K. Hoffman, J. Hubbard, R. Oliva, and W. Weckesser, *ibid.* **2**, 570 (2003).
- ⁶³T. Vo and M. Wechselberger, *SIAM J. Math. An.* **47**, 3235 (2015).
- ⁶⁴J. Burke, M. Desroches, A. Granados, T.J. Kaper, M. Krupa, and T. Vo, *J. Nonlin. Sci.* **26**, 405 (2016).
- ⁶⁵P. Szmolyan and M. Wechselberger, *J. Diff. Eq.* **200**, 69 (2004).
- ⁶⁶X. Han and Q. Bi, *Nonlinear Dynamics* **68**, 275 (2012).
- ⁶⁷The kinetics in (1) are equivalent to the classical $x_t = y - (\frac{1}{3}x^3 - x)$, $y_t = \varepsilon(\tilde{a} - x + b \cos(\theta))$ under the linear shift $u = x - 1$, $v = y + \frac{2}{3}$, and $a = \tilde{a} - 1$.
- ⁶⁸F. Buchholtz, M. Dolnik, and I.R. Epstein, *J. Phys. Chem.* **99**, 15093 (1995).
- ⁶⁹W. Teka, J. Tabak, T. Vo, M. Wechselberger, and R. Bertram, *J. Math. Neuro.* **1**, 12 (2011).
- ⁷⁰M. Wechselberger, J. Mitry, and J. Rinzel, in *Nonautonomous Dynamical Systems in the Life Sciences*, **LNMB 2012**, Springer, 89 (2013). J. Mitry and M. Wechselberger, *SIAM J. Appl. Dyn. Sys.* **16**, 546 (2017).
- ⁷¹M. Krupa, B. Ambrosio, and M.A. Aziz-Alaouio, *Nonlinearity* **27**, 1555 (2014).
- ⁷²K.-L. Roberts, J.E. Rubin, and M. Wechselberger, *SIAM J. Appl. Dyn. Sys.* **14**, 1808 (2015).
- ⁷³E. Bossolini, M. Brøns, and K. Uldall-Kristiansen, *SIAM Rev.* **62**, 869 (2020).
- ⁷⁴M. Brøns and K. Bar-Eli, *J. Phys. Chem* **95**, 8706 (1991).
- ⁷⁵P. de Maesschalck, E. Kutafina, and N. Popovic, *J. Dyn. Diff. Eq.* **26**, 955 (2014).
- ⁷⁶M. Wechselberger, *SIAM J. Appl. Dyn. Sys.* **4**, 101 (2005). M. Krupa and M. Wechselberger, *J. Diff. Eq.* **248**, 2841 (2010).
- ⁷⁷The local minimum of the critical manifold $\{(u, v, \theta) | v = u^2 + \frac{1}{3}u^3\}$, for $\varepsilon = 0$. On this manifold, the reduced flow is $u(u+2)\dot{u} = a - u + b \cos(\theta)$ and $\dot{\theta} = \omega$, as derived by taking $\frac{d}{dt}$ of the algebraic equation defining the manifold. The regular FN dynamics occur for $b^2 < a^2 + \frac{1}{64\omega^2}$.
- ⁷⁸E. Benoit, J. L. Callot, F. Diener, and M. Diener, *Collectanea Mathematica* **31**, 3 (1980). W. Eckhaus, in *Lecture Notes in Math.* **985**, Springer-Verlag, 449 (1983). A.K. Zvonkin and M.A. Shubin, *Russ. Math. Surv.* **39**, 69 (1984). M. Brøns, in *Proc. 9th AIMS Intl. Conf., Disc. Cont. Dyn. Sys., Suppl.* **77-83** (2013).
- ⁷⁹T.J. Kaper and T. Vo, *Chaos* **28**, 091103 (2018).
- ⁸⁰R. Goh, T.J. Kaper, and T. Vo, ArXiv DS:2012.10048 (2020).
- ⁸¹D. Avitabile, M. Desroches, R. Veltz, and M. Wechselberger, *SIAM J. Math. An.* **52**, 5703 (2020).
- ⁸²T. Vo, R. Bertram, and T. J. Kaper, *Physica D* **411**, 132544 (2020).